Enhanced single-cell printing by acoustophoretic cell focusing

I. Leibacher,[1,a),b)] J. Schoendube,[2,3,a),b)] J. Dual,[1] R. Zengerle,[2,4,5] and P. Koltay[2,6]
[1]*Institute of Mechanical Systems, Department of Mechanical and Process Engineering, Swiss Federal Institute of Technology (ETH), Tannenstr. 3, CH-8092 Zurich, Switzerland*
[2]*Laboratory for MEMS Applications, Department of Microsystems Engineering-IMTEK, University of Freiburg, Georges-Koehler-Allee 103, 79110 Freiburg, Germany*
[3]*cytena GmbH, Georges-Koehler-Allee 103, 79110 Freiburg, Germany*
[4]*HSG-IMIT, Georges-Koehler-Allee 103, 79110 Freiburg, Germany*
[5]*BIOSS Centre for Biological Signalling Studies, University of Freiburg, 79110 Freiburg, Germany*
[6]*BioFluidiX GmbH, Georges-Koehler-Allee 103, 79110 Freiburg, Germany*

(Received 16 February 2015; accepted 23 March 2015; published online 31 March 2015)

Recent years have witnessed a strong trend towards analysis of single-cells. To access and handle single-cells, many new tools are needed and have partly been developed. Here, we present an improved version of a single-cell printer which is able to deliver individual single cells and beads encapsulated in free-flying picoliter droplets at a single-bead efficiency of 96% and with a throughput of more than 10 beads per minute. By integration of acoustophoretic focusing, the cells could be focused in x and y direction. This way, the cells were lined-up in front of a 40 μm nozzle, where they were analyzed individually by an optical system prior to printing. In agreement with acoustic simulations, the focusing of 10 μm beads and Raji cells has been achieved with an efficiency of 99% (beads) and 86% (Raji cells) to a 40 μm wide center region in the 1 mm wide microfluidic channel. This enabled improved optical analysis and reduced bead losses. The loss of beads that ended up in the waste (because printing them as single beads arrangements could not be ensured) was reduced from 52% $\pm$ 6% to 28% $\pm$ 1%. The piezoelectric transducer employed for cell focusing could be positioned on an outer part of the device, which proves the acoustophoretic focusing to be versatile and adaptable. [http://dx.doi.org/10.1063/1.4916780]

I. INTRODUCTION

Within the last decade, microfluidic handling of cells has experienced a growing interest towards the single-cell level. One approach to provide single cells for subsequent analysis is based on single-cell printing. Contributing to these developments, the article at hand presents the combination of a microfluidic single-cell printing device[1,2] with acoustophoretic particle focusing. Focusing of particles/cells led to a more reliable particle detection and processing within the biomicrofluidic system.

In microfluidic devices, the focusing of particles/cells into a tightly focused stream along a channel centerline is a common step prior to various counting, detecting, and sorting tasks. Prime examples are flow cytometers and fluorescence-activated cell sorting (FACS), whose performances rely on the focusing of the particles/cells suspended in a carrier fluid. In such devices, focusing is commonly achieved by hydrodynamic focusing.[3] More general, literature

[a)]I. Leibacher and J. Schoendube contributed equally to this work and were listed in alphabetical order.
[b)]Authors to whom correspondence should be addressed. Electronic addresses: leibacher@imes.mavt.ethz.ch and jonas.schoendube@imtek.de

describes many different methods for particle focusing[4] that can be classified into sheath flow focusing (e.g., the mentioned hydrodynamic focusing[5]) and sheathless focusing (e.g., with dielectrophoretic,[6] hydrophoretic,[7] inertial,[8] optical,[9] or acoustic[10–12] forces).

In this article, we apply focusing by acoustophoresis[13,14] which has previously been demonstrated in a range of applications[15] from focusing[10–12] to cell separation and sorting,[16,17] trapping,[18] and elution.[19] Acoustophoresis offers several benefits for the considered purpose: It works efficiently for a wide range of particle properties and flow conditions, it is simple to implement on an existing microfluidic chip without any on-chip modifications, and it does not require a large instrumentation overhead. Compared to this approach, the common hydrodynamic focusing has two main drawbacks: Particles can only be focused with fluid flow, which is not always present in a drop-on-demand dispenser, and the required sheath flows dilute the particle concentration and increase the device complexity. For the intended focusing, other particle handling methods are also at a disadvantage: Dielectrophoresis requires elaborate in-chip electrodes, inertial focusing operates with high flow speeds, and optical tweezers feature a complex optical setup.

The acoustic focusing is integrated with a single-cell printing device as published earlier.[1,2] This device and technology, referred to as "single-cell printer (SCP)," enables the controlled, non-contact, inkjet-like printing of single cells onto defined positions on a variety of substrates with exactly one cell per microdroplet.

The SCP is particularly suited to conduct single-cell studies in fields such as stem cell biology, hematology, cancer biology, or tissue engineering. Compared to FACS, the SCP is particularly suited for rare and single-cell handling in terms of cell viability, set-up time, and low sample volumes.[2] The SCP features a disposable inkjet-like cartridge (avoids cross-contamination), image-based cell detection (rather than lasers) without fluorescent labelling and a gentle, targeted dispensing mechanism (rather than continuous jetting and charging of droplets in FACS).

In the central element of the SCP—the dispenser chip, cells are flowing through a microfluidic channel towards a nozzle, where they are expelled one by one. When cells are flowing in a non-focused manner, the integrated optical particle detection system is not able to unambiguously identify all cells in order to be printed properly. Therefore, some cells are lost and cannot be printed onto the substrate. This cell loss in the detection step can be improved by acoustophoretic focusing of the cells within the channel. The focusing offers two more improvements: (1) Focused particles may allow a higher speed of the image processing, hence the throughput increases, and (2) focused particles have a defined, uniform position and flow velocity at the nozzle, which leads to a more predictable cell dispensation behavior of the SCP.

Acoustophoretic focusing on the SCP is described experimentally, numerically, and in terms of printing performance. Relevance of the focusing approach with outer placement of the piezoelectric transducer is expected for many further particle handling systems.

II. METHODS AND BACKGROUND

A. Experimental setup: The single-cell printer

The SCP consists of a three-axis lab robot, a picoliter droplet generator, and a camera with optics. The camera images the nozzle area of the dispenser chip and a fully automated object recognition algorithm detects cells in a region of interest (ROI, dashed line Fig. 1). For every dispense, the liquid volume within the ROI is ejected as a free flying droplet. If a single cell is detected within the ROI, the cell can be printed onto a substrate of choice (typically microwell plates or glass slides). When no cell or multiple cells are detected in the ROI, still a droplet is dispensed, but a vacuum shutter deflects the non-conforming droplets in flight into a waste system.

For a problem statement, Figs. 2(a) and 2(b) show two time series images as they were processed by the detection algorithm of the SCP. In each image row, a polystyrene bead (as a surrogate for a cell) in aqueous medium is moving closer towards the nozzle with each dispensed droplet, before the bead itself reaches the ROI and is finally expelled from the nozzle in the subsequent dispense. Without focusing, the beads are randomly distributed within the

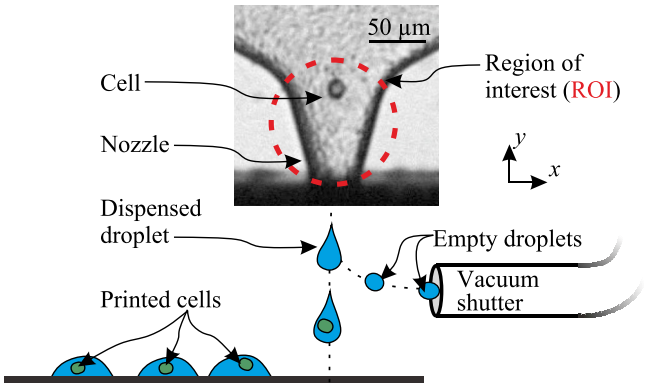

FIG. 1. Principle of the SCP: A drop-on-demand dispenser prints beads or cells in aqueous droplets through a nozzle. An image detection system with shown ROI controls that empty droplets and droplets with multiple cells are sucked into a waste system, so only droplets with exactly one cell reach the target.

dispenser chip. Most of the time, beads in the channel center are successfully detected and printed (Fig. 2(a)). However, beads close to the channel wall (Fig. 2(b)) have a reduced contrast to the background: An approximately 5-10 μm wide shadowy band along the channel walls cannot readily be avoided by the coaxial illumination. The beads in this band are not properly detected by the recognition algorithm because of the shadow and because they are flowing slower than the centered particles. Such detection errors contribute to a detection and printing yield of the SCP below 100%, which is especially adverse in the case of rare cell printing.

In order to reduce these detection errors, we propose the focusing of the particles in x-direction onto the channel centerline by means of acoustophoresis as illustrated in Fig. 3. For the actuation of an acoustophoretic resonance mode, a piezoelectric transducer (thickness 1 mm, Ferroperm piezoceramics Pz26, size 5 mm $\times$ 2.5 mm) was glued on the PMMA housing of the chip with conductive epoxy (Epo-Tek H20E; in some earlier experiments directly glued on the back side of the silicon channel). For the experiments, the piezoelectric transducer was excited by a function generator (Agilent 33120A) connected to a radiofrequency power amplifier (E&I 325LA) with a resulting excitation voltage of 17.5 V_{rms} at frequencies around 0.5–1.5 MHz.

The microfluidic dispenser chip itself was fabricated from a silicon wafer (thickness 300 μm). In the silicon substrate, a fluidic channel (blue in Fig. 3(a)) was dry etched 40 μm

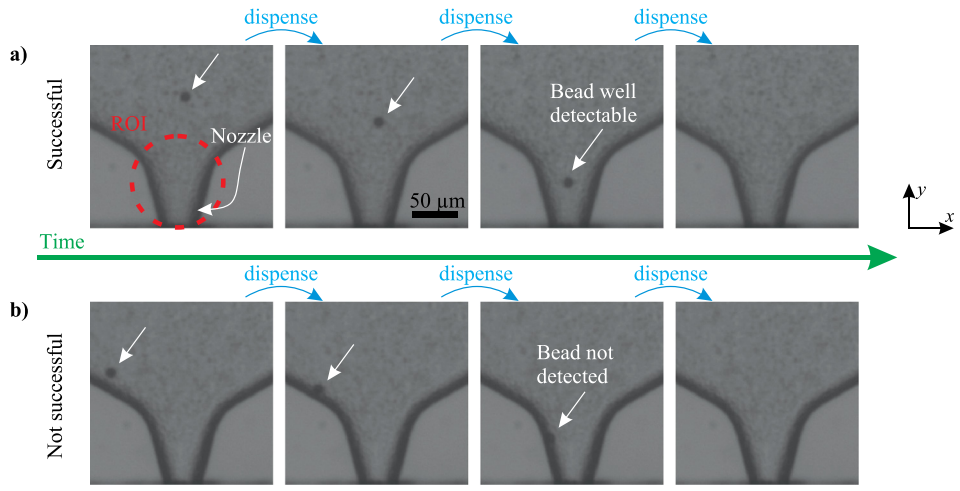

FIG. 2. Problem statement: (a) Raw image series of a well detectable cell-sized bead (10 μm), passing through the region of interest in the nozzle center right before its dispensation. (b) A bead that was not detected by the detection algorithm, because it passed through the shadow area close to the channel wall.

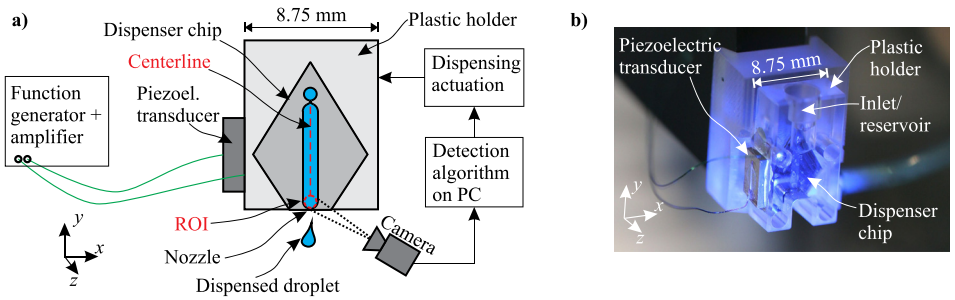

FIG. 3. (a) Schematic of the experimental setup for acoustophoretic focusing of cells on the centerline within the dispenser chip. (b) Photograph of the illustrated setup.

deep by an ICP system. The channel has a maximal width of 1 mm in x-direction and a length of 6 mm in y-direction. The channel was sealed by anodic bonding with a Pyrex glass wafer (thickness 300 μm), featuring etched inlet holes. This dispenser chip was glued into a milled plastic holder (PMMA), which provides an inlet and reservoir for the cell suspension. The chip holder is mechanically clamped to a dispenser module (P9, BioFluidiX GmbH). For the droplet dispensation, a second piezoelectric actuator can deflect the silicon membrane on the back side of the chip on demand in z-direction. The membrane deflection causes a volume displacement which in turn leads to the dispensation of a picoliter droplet through the nozzle. The dispenser was filled with a cell or bead suspension ($5 \cdot 10^5\,\mathrm{ml}^{-1}$) by means of a syringe.

B. Theoretical background: Acoustophoretic focusing

The theory of acoustophoresis is well described in literature.[20–22] Here, we will limit the theoretical background to the equations necessary for the understanding of later experimental results. We assume particles that are suspended in a water-filled microfluidic channel. For the focusing of particles towards the channel centerline, a half wavelength of a standing pressure wave is necessary across the channel width $w = \lambda/2$ (also called $\lambda/2$ mode). Its first-order pressure field p_1 reads

$$p_1(x,t) = p_\mathrm{A} \cos(kx) \sin(2\pi f_\mathrm{a} t), \tag{1}$$

with the pressure amplitude p_A, the wave number $k = 2\pi/\lambda$, the spatial coordinate x in width direction of the channel, the acoustic frequency f_a of the excitation, and the time t. This is a reasonable first 1D approximation since the channel is much longer in y-direction than wide in x-direction, and its height in z-direction is much smaller than half the wavelength.

For the calculation of the acoustic radiation force $\vec{F}$ on a particle of radius $r_\mathrm{p} \ll \lambda$ in this field, we use the Gor'kov potential[22] U with $\vec{F} = -\nabla U$

$$U = \pi r_\mathrm{p}^3 \left(\frac{2}{3} \kappa_\mathrm{wa} f_1 \langle p_1^2 \rangle - \rho_\mathrm{wa} f_2 \langle v_1^2 \rangle \right), \tag{2}$$

with the particle-dependent factors

$$f_1 = 1 - \frac{\kappa_\mathrm{p}}{\kappa_\mathrm{wa}}, \quad f_2 = \frac{2(\rho_\mathrm{p} - \rho_\mathrm{wa})}{2\rho_\mathrm{p} + \rho_\mathrm{wa}}, \tag{3}$$

with the particle (index "p") and medium (here water, index "wa") compressibilities and densities κ and ρ. The velocity field $v_1 = \|\vec{v_1}\|$ follows from linear acoustics.[20] In the channel, with the one-dimensional approximation, the force on a particle then yields[21]

$$F = \vec{F} \cdot \vec{e}_x = 4\pi \Phi k r_\mathrm{p}^3 E_\mathrm{a} \sin(2kx), \tag{4}$$

with the acoustic contrast factor $\Phi = f_1/3 + f_2/2$ and the acoustic energy density $E_a = p_A^2/(4\rho_{wa}c_{wa}^2)$ for the speed of sound c_{wa} in water. Particles with $\Phi > 0$ (such as cells and copolymer/polystyrene test beads) will be attracted to the central pressure nodal line at $x = w/2$.

Ideally, the resonance is generated by choosing the excitation frequency to be exactly the first resonance frequency $f_a = c_{wa}/\lambda = c_{wa}/(2w)$ of the channel. However, in experiments, the resonance frequency varies from device to device because of manufacturing imperfections and compliance of the channel walls, as also discussed in Sec. III A. It also varies at different locations along the channel. Additionally, the resonance frequency was reported to change $\sim$1 kHz per degree of temperature change.[23] This is problematic due to varying ambient temperatures and especially when device heating occurs from the applied power on the transducer. To overcome these problems, the excitation frequency can be modulated around the resonance frequency, which results in a more robust and tighter focusing of the particles on the channel centerline.[24] By modulating the frequency, a broad range of frequencies will be excited. As long as the precise resonance frequency lies within this range, the particles will focus.

Another acoustofluidic effect is the particle-particle interaction in an acoustic field. These secondary forces are known as "Bjerknes forces."[17] Depending on the material properties of the particles and the suspending liquid, Bjerknes forces can be either attractive (bringing two particles together) or repulsive. Generally, for two particles of similar material properties, the Bjerknes force is attractive. However, in our applied experiments with cells, we did not observe influences of Bjerknes forces, as they might be too small in our setting.

With regard to cell viability, acoustophoresis is known to be a gentle method. Viability-related effects such as cavitation, thermal stress, and acoustic streaming are well-studied and have been discussed in a recent review.[25] Several research groups reported on acoustophoretic cell handling with no adverse effects on cell viability, where cells were exposed up to 72 h in a MHz ultrasonic field in microfluidic devices.[18,26] Compared to these studies, in our application, the cells are exposed to the ultrasonic field for a much shorter time of only about 1 min, which allays viability concerns. Regarding the cell viability of the cell printer itself, a high post-printing viability for several cell types has been documented previously.[1,2] Therefore, we assume the cell viability not to be a key point in our study.

III. RESULTS

A. Acoustophoretic characterization

A characterization of the acoustophoretic device behavior will be given here for the understanding of the following applications.

The 1 mm $\times$ 40 μm rectangular cross-section of the microfluidic channel in x- and z- directions is well-suited for acoustophoresis. However, regarding the y-direction, the rounded inlet and nozzle might have a disturbing influence on the acoustic fields. To find out about these effects, we simulated the acoustic eigenmode of the channel numerically in 2D with Comsol Multiphysics® (pressure acoustics module, eigenfrequency analysis) like shown in Fig. 4. The simulation consists of an acoustic domain of the water channel geometry, where the high difference of the characteristic acoustic impedance at the water-silicon interface is modeled with hard-wall boundary conditions all around.[20,27] The water properties[20] are $c_{wa} = 1497$ m/s, $\rho_{wa} = 998$ kg/m^3 at 25 °C.

We focus on the first and second resonance ($\lambda/2$ and λ) modes in x-direction, which result in a focusing of the particles on one and two vertical lines, respectively. The first resonance mode will be the relevant mode for our application. With the simplified calculation of $f_a = c_{wa}/\lambda$, we expected these modes to occur at 749 kHz and 1497 kHz, which matches well to the simulation results of 755 kHz and 1503 kHz. Unlike the analytical 1D assumption of Sec. II B, the acoustic fields turn out to be slightly dependent on y as they decay towards the inlet and the nozzle.

The Gor'kov potential U is also plotted in Fig. 4 for copolymer beads. Their acoustophoretic behavior is similar to the behavior of cells, since the density $\rho_{co} = 1050$ kg/m^3 of

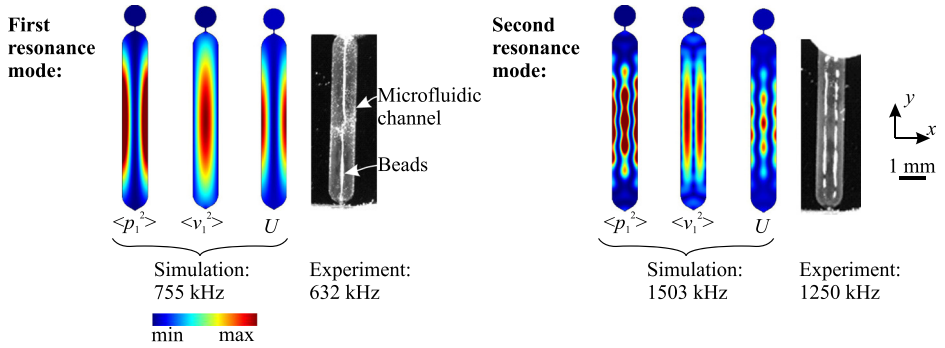

FIG. 4. Resonance modes in the microfluidic channel: numerical simulations (pressure field, velocity field, and Gor'kov potential U) in comparison to the experimental results. The vertical white lines are 11 μm copolymer beads which were attracted to the minimal potential U in the channel.

copolymer is similar to cell densities and their compressibility is also lower than the compressibility of water. The parameters for copolymer beads[28] are $f_1 = 0.76$ and $f_2 = 0.034$. $f_2 \ll 1$ denotes an almost negligible influence of the velocity term in Eq. (2), and $f_1 > 0$ leads to an attraction of particles to the pressure minima, which is reflected by the similarity of the fields for $\langle p_1^2 \rangle$ and U. Interpreting the Gor'kov potential U, particles will get attracted to the blue minima of this potential field, whereas the acoustic radiation forces are higher in the middle of the channel with regard to the y-direction, because of higher slopes of the pressure field in x-direction. The maximum of the velocity field $\langle v_1^2 \rangle$ in the channel center causes an undesired attraction of the particles towards this center in y-direction; however, this effect was not observed experimentally due to the negligible influence of the velocity field as denoted by the small f_2 value. In conclusion, the channel geometry allows for the generation of a suitable pressure field for particle focusing along the centerline of the dispenser chip, despite the rounded corners at the channel ends.

The resonance frequency values in the experiment were found to be 632 kHz and 1250 kHz, which are 83.7% and 83.2% of the value from the numerical simulations. This difference between the numerical simulation and the experiment is possibly caused by several simplifications: First, the silicon boundaries are not a perfect hard-wall boundary, but rather compliant boundaries with non-zero wave transmission from the water into the silicon wall.[27] A modeling of this wall compliance with a lossy-wall/impedance boundary condition[20] could yield a better match with the experiment. Second, the simplification of the complex 3D fluid-structure interaction problem with coupled physics to a 2D problem gives a simulation domain which is much stiffer than the real model. The elastic PMMA holder and the glued piezoelectric transducer further influence the resonance mode. Nevertheless, the qualitative insight into the acoustic fields is valuable for the understanding of the acoustic radiation forces.

In Fig. 5, the particle patterns of further resonance modes are shown. These resonance modes remind of the particle patterns in the famous Chladni figures.[29] Many of them cannot be employed for applications or they can even interfere with the focusing; however, the resonance mode in Fig. 5(a) is of interest. It might be employed, e.g., for particle handling tasks such as the particle trapping against a flow in y-direction, for the grouping of particles, or for

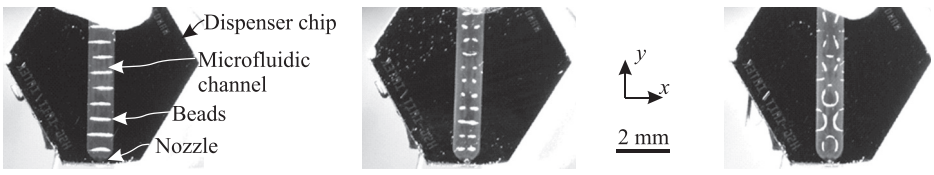

FIG. 5. 2D resonance modes in the microfluidic channel, resembling Chladni figures.

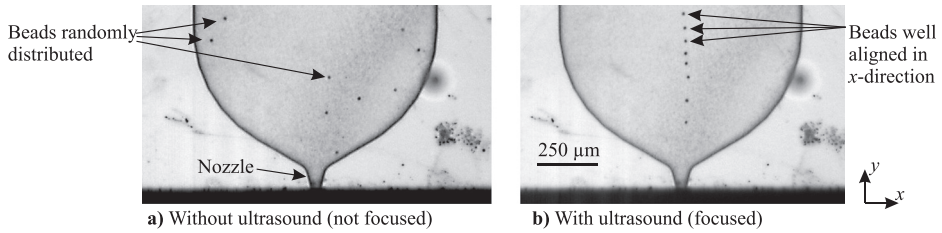

FIG. 6. Alignment of cell-like beads (10 μm polystyrene) on the vertical channel centerline for enhanced printing performance (Multimedia view). [URL: http://dx.doi.org/10.1063/1.4916780.1] The excitation of the piezoelectric transducer had a carrier frequency of 630 kHz and was modulated with a deviation of ± 10 kHz. Frequency modulation showed to result in robust and stable focusing.

the dispensation of cell-free buffer to pre-fill a substrate before actual single-cell printing. The numerical simulation also predicted many eigenmodes resembling the Chladni figures; however, the more complex the pattern, the more sensitive it reacts to parameter differences between the numerical model and the experiment.

B. Printing evaluation

This chapter compares the SCP printing performance with and without acoustophoretic focusing.

Fig. 6(a) (multimedia view) shows a random distribution of beads in the dispenser chip during printing as known from earlier experiments. When the piezoelectric transducer was turned on, the beads aligned along the *y*-axis (Fig. 6(b), multimedia view) within a couple of seconds. For the acoustic excitation, a carrier frequency of 630 kHz was modulated sinusoidally with 1 Hz and a deviation of ± 10 kHz. As expected, this modulation increased the robustness of the focusing, thus no finetuning of the resonance frequency was necessary even during long series of focusing experiments on several device specimen. After the acoustophoretic alignment, the beads were transported stepwise with each dispensation towards the nozzle. Due to laminar flow conditions, the bead alignment in the channel was preserved during dispensation. Therefore, the transducer can be turned off after a focusing of all beads in the channel until newly entered, non-focused beads reach the nozzle. Turning off the transducer is beneficial for reduced transducer heating and reduced power consumption.

Quantifying the focusing, in Fig. 7, the experimentally determined probability of bead/cell locations is plotted over the *x*-axis. The *x*-position of the beads/cells was measured at the 1 mm wide section of the microfluidic channel. Without focusing, 10 μm beads were distributed equally. With focusing, the plot shows that 99% of the beads were confined to a 40 μm wide

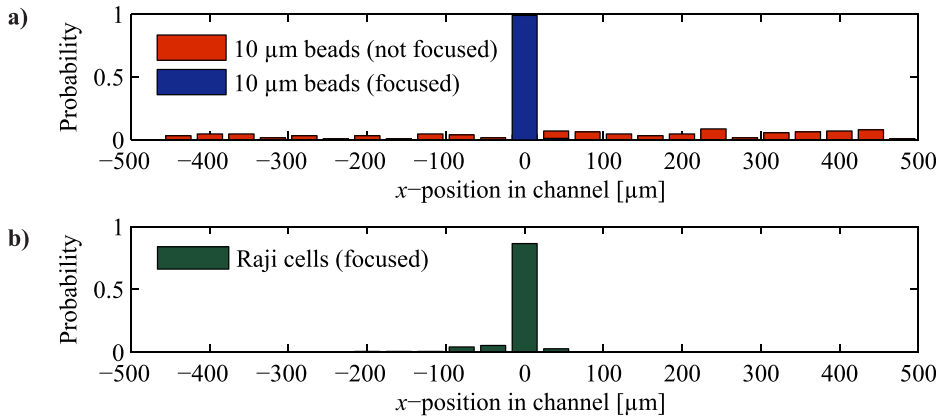

FIG. 7. Histogram of the bead locations in the microfluidic channel.

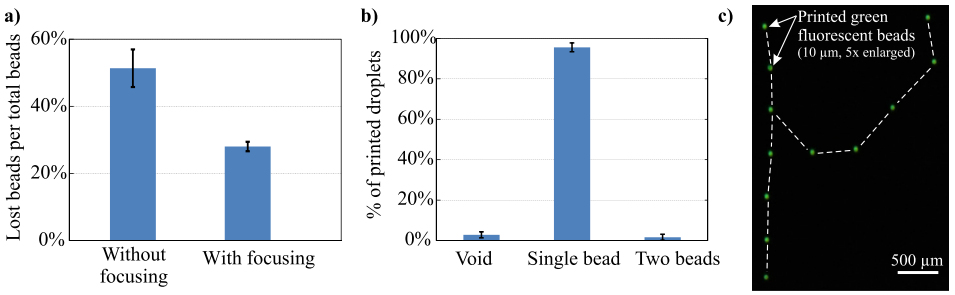

FIG. 8. (a) Statistical evaluation of the printing performance (N = 670 beads, error bars correspond to standard deviations). (b) The percentage of droplets dispensed on the substrate with exactly one single bead was 95.6%. (c) As demonstration of the correct printing performance with acoustophoretic focusing, a "μ" has been printed with 10 μm fluorescent beads (enlarged 5 × for visibility).

center region of the channel. In a next step, focusing of cells has been evaluated with Raji cells. Raji cells are derived from human B-lymphocytes and are therefore of particular interest in the field of antibody screening.[30] As also plotted in Fig. 7, Raji cells have been focused with an efficiency of 86% to the mentioned center region and were successfully dispensed. The focusing of cells is slightly less tight than the focusing of beads, probably due to a lower Φ and size variations.

For further quantification, the effect of focusing on the percentage of lost beads has been studied. This percentage quantifies the amount of lost beads (sucked into waste) in relation to the total number of beads that passed the nozzle. Fig. 8(a) shows a reduction of this value from 52% ± 6% to 28% ± 1%. In total, 670 polystyrene beads have been dispensed at a throughput of more than 10 beads per minute. Without focusing 195 out of 406 beads, with focusing 190 out of 264 beads, have been successfully detected and dispensed individually. This performance increase is attributed to the enhanced detection of beads by the algorithm when they were aligned in the center of the nozzle. The remaining bead loss is largely due to the fact that sometimes two or more beads arrive at the nozzle coincidentally. In this case, the droplets are sucked into the waste system, as required for single-cell applications. This loss can be reduced by lowering the concentration of beads at the cost of longer processing time.

The acoustophoretic printing performance was further studied by determining the single-bead efficiency in Fig. 8(b). The single-bead efficiency is defined as the percentage of droplets which were correctly printed onto the substrate containing exactly one bead. The single-bead efficiency was 95.6% ± 2.2% (N = 400), with only 2.8% ± 1.5% void droplets and 1.6% ± 1.5% droplets with two beads. These results are in accordance with previously reported single-cell efficiencies.[1,2]

Finally, to demonstrate that the acoustic focusing is not influencing the droplet trajectory and precise printing is possible, fluorescently labeled 10 μm beads were printed on a glass slide. Fig. 8(c) shows a micrograph of this glass slide, where 12 bead positions form the letter "μ."

IV. CONCLUSION

The performance improvement of a single-cell printing device by acoustophoretic focusing has been described. In the experiments with beads and Raji cells, acoustophoretic focusing showed to increase the device performance significantly: The bead loss was reduced from 52% ± 6% to 28% ± 1%. This performance increase is crucial for many single-cell analysis applications, where cells of interest are rare. The focusing might also lead to increased cell printing throughput, as it allows for reduction of the ROI image size which enables a faster processing of the computationally intense cell detection algorithm, which is currently a rate limiting component of the setup. A high single-bead printing efficiency (95.6% ± 2.2%) and correct droplet positioning were demonstrated similar to the performance of the device when no focusing is applied.

Regarding the acoustophoretic focusing, the attachment of the piezoelectric transducer on the plastic chip holder was found to be well suited. This attachment is different from previous work in literature, where the transducer is usually placed directly on the chip in the proximity of the microfluidic channels,[31] or directly at the outside in the case of capillary type devices.[32] In our design, the piezoelectric transducer excites a coupled structure-fluid resonance which also includes the plastic chip holder. Even though the vibration of the chip holder implicates damping of the transducer's energy, a high pressure amplitude suitable for acoustophoresis could be induced in the microchannel. Therefore, the proposed transducer attachment offers several advantages compared to the on-chip placement: The commonly experienced problem of chip heating by the transducer power can be solved, which is especially important for the handling of cells. A second advantage is the freedom in the geometrical placement of the transducer, which is of increased interest for more complex lab-on-a-chip systems with limited installation space on the chip itself.

Furthermore, frequency modulation showed to result in a stable focusing of the particles. Frequency modulation could compensate disturbances which lead to resonance frequency shifts, therefore no acoustophoretic parameter adjustments were necessary even during long series of focusing experiments.

The presented focusing method showed to be simple in instrumentation, low cost in terms of fabrication, and it worked reliably in a robust manner. Therefore, the insights of this paper might contribute to or inspire similar focusing approaches, which could improve the performance of a wide range of biomicrofluidic devices.

ACKNOWLEDGMENTS

The authors would like to express their gratitude for funding by ETH Zurich and the European Commission (Project PASCA, www.pasca.eu, FP7 GA257073). J.S. and I.L. are inventors on a patent application related to the reported approach. J.S., P.K., and R.Z. have equity interests in cytena GmbH, a company that is developing single-cell analysis and handling solutions.

[1]A. Yusof, H. Keegan, C. D. Spillane, O. M. Sheils, C. M. Martin, J. J. O'Leary, R. Zengerle, and P. Koltay, Lab Chip **11**, 2447 (2011).
[2]A. Gross, J. Schöndube, S. Niekrawitz, W. Streule, L. Riegger, R. Zengerle, and P. Koltay, J. Lab. Autom. **18**, 504 (2013).
[3]D. Ateya, J. Erickson, P. Howell, L. Hilliard, J. Golden, and F. Ligler, Anal. Bioanal. Chem. **391**, 1485 (2008).
[4]X. Xuan, J. Zhu, and C. Church, Microfluid. Nanofluid. **9**, 1 (2010).
[5]G.-B. Lee, C.-C. Chang, S.-B. Huang, and R.-J. Yang, J. Micromech. Microeng. **16**, 1024 (2006).
[6]H. Chu, I. Doh, and Y.-H. Cho, Lab Chip **9**, 686 (2009).
[7]S. Choi and J.-K. Park, Anal. Chem. **80**, 3035 (2008).
[8]D. Di Carlo, D. Irimia, R. G. Tompkins, and M. Toner, Proc. Natl. Acad. Sci. USA **104**, 18892 (2007).
[9]Y. Zhao, B. S. Fujimoto, G. D. Jeffries, P. G. Schiro, and D. T. Chiu, Opt. Express **15**, 6167 (2007).
[10]Lifetechnologies, "Attune(r) acoustic focusing cytometer," www.lifetechnologies.com.
[11]M. Ward, P. Turner, M. DeJohn, and G. Kaduchak, "Fundamentals of acoustic cytometry," in *Current Protocols in Cytometry* (John Wiley & Sons, Inc., 2001).
[12]M. E. Piyasena, P. P. Austin Suthanthiraraj, R. W. Applegate, A. M. Goumas, T. A. Woods, G. P. López, and S. W. Graves, Anal. Chem. **84**, 1831 (2012).
[13]R. Barnkob, P. Augustsson, T. Laurell, and H. Bruus, Lab Chip **10**, 563 (2010).
[14]H. Bruus, J. Dual, J. Hawkes, M. Hill, T. Laurell, J. Nilsson, S. Radel, S. Sadhal, and M. Wiklund, Lab Chip **11**, 3579 (2011).
[15]A. Lenshof, C. Magnusson, and T. Laurell, Lab Chip **12**, 1210 (2012).
[16]F. Petersson, L. Åberg, A.-M. Swärd-Nilsson, and T. Laurell, Anal. Chem. **79**, 5117 (2007).
[17]T. Laurell, F. Petersson, and A. Nilsson, Chem. Soc. Rev. **36**, 492 (2007).
[18]M. Evander and J. Nilsson, Lab Chip **12**, 4667 (2012).
[19]P. Augustsson, J. Malm, and S. Ekström, Biomicrofluidics **6**, 034115 (2012).
[20]H. Bruus, Lab Chip **12**, 20 (2012).
[21]H. Bruus, Lab Chip **12**, 1014 (2012).
[22]L. P. Gor'kov, Sov. Phys.-Doklady **6**(9), 773 (1962).
[23]P. Augustsson, R. Barnkob, S. T. Wereley, H. Bruus, and T. Laurell, Lab Chip **11**, 4152 (2011).
[24]O. Manneberg, B. Vanherberghen, B. Onfelt, and M. Wiklund, Lab Chip **9**, 833 (2009).
[25]M. Wiklund, Lab Chip **12**, 2018 (2012).

[26]B. Vanherberghen, O. Manneberg, A. Christakou, T. Frisk, M. Ohlin, H. M. Hertz, B. Onfelt, and M. Wiklund, Lab Chip **10**, 2727 (2010).
[27]I. Leibacher, S. Schatzer, and J. Dual, Lab Chip **14**, 463 (2014).
[28]S. Oberti, A. Neild, and J. Dual, J. Acoust. Soc. Am. **121**, 778 (2007).
[29]I. Leibacher and J. Dual, Proceedings of the 2013 International Congress on Ultrasonics (ICU 2013), 2nd–5th May 2013, Singapore, 2013.
[30]A. M. Clargo, A. R. Hudson, W. Ndlovu, R. J. Wootton, L. A. Cremin, V. L. O'Dowd, C. R. Nowosad, D. O. Starkie, S. P. Shaw, J. E. Compson *et al*., in *mAbs* (Landes Bioscience, 2013) , Vol. 6, pp. 143–159.
[31]A. Lenshof, M. Evander, T. Laurell, and J. Nilsson, Lab Chip **12**, 684 (2012).
[32]B. Hammarström, M. Evander, H. Barbeau, M. Bruzelius, J. Larsson, T. Laurell, and J. Nilsson, Lab Chip **10**, 2251 (2010).